Virus Research 344 (2024) 199359

Contents lists available at ScienceDirect

Virus Research

journal homepage: www.elsevier.com/locate/virusres

Discovery of a potent inhibitor, **D-132**, targeting *AsfvPolX*, via protein-DNA complex-guided pharmacophore screening and in vitro molecular characterizations

Yi-Chen Wu [a,1], Hui-Xiang Lai [a,1], Ji-Min Li [b,c,1], Kit-Man Fung [d], Tien-Sheng Tseng [a,*]

[a] *Institute of Molecular Biology, National Chung Hsing University, Taichung, 40202, Taiwan*
[b] *Institute of Precision Medicine, College of Medicine, National Sun Yat-sen University, Kaohsiung, 80424, Taiwan*
[c] *Center of Excellence for Metabolic Associated Fatty Liver Disease, National Sun Yat-sen University, Kaohsiung, 80424, Taiwan*
[d] *Biomedical Translation Research Center (BioTReC), Academia Sinica, Taipei, 11529, Taiwan*

ARTICLE INFO

Keywords:
ASFV
*Asfv*PolX
Pharmacophore-based inhibitor screening
Drug discovery
Fluorescence polarization
LSPR
Molecular docking
Antiviral inhibitor

ABSTRACT

The heightened transmissibility and capacity of African swine fever virus (ASFV) induce fatal diseases in domestic pigs and wild boars, posing significant economic repercussions and global threats. Despite extensive research efforts, the development of potent vaccines or treatments for ASFV remains a persistent challenge. Recently, inhibiting the *Asfv*PolX, a key DNA repair enzyme, emerges as a feasible strategy to disrupt viral replication and control ASFV infections. In this study, a comprehensive approach involving pharmacophore-based inhibitor screening, coupled with biochemical and biophysical analyses, were implemented to identify, characterize, and validate potential inhibitors targeting *Asfv*PolX. The constructed pharmacophore model, **Phar-PolX-S**, demonstrated efficacy in identifying a potent inhibitor, **D-132** (IC_{50} = 2.8 ± 0.2 μM), disrupting the formation of the *Asfv*PolX-DNA complex. Notably, **D-132** exhibited strong binding to *Asfv*PolX (KD = 6.9 ± 2.2 μM) through a slow-on-fast-off binding mechanism. Employing molecular modeling, it was elucidated that **D-132** predominantly binds in-between the palm and finger domains of *Asfv*PolX, with crucial residues (R42, N48, Q98, E100, F102, and F116) identified as hotspots for structure-based inhibitor optimization. Distinctively characterized by a 1,2,5,6-tetrathiocane with modifications at the 3 and 8 positions involving ethanesulfonates, **D-132** holds considerable promise as a lead compound for the development of innovative agents to combat ASFV infections.

1. Introduction

The African swine fever virus (ASFV) presents a formidable menace owing to its heightened transmissibility and capacity to instigate fatal ailments in domestic pigs and wild boars alike (Tulman et al., 2009). Initially confined to Africa until 1957, ASFV has disseminated extensively, reaching various European nations, the Caribbean, and Asia, thereby instigating notable economic ramifications in specific locales (Choi et al., 2021b; Vinuela, 1985). The substantial culling initiative in Cuba during 1971, involving over 500,000 pigs, aimed to avert a nationwide animal epidemic and gained international recognition as the preeminent event of concern by the United Nations Food and Agricultural Organization (Costard et al., 2013; Yoo et al., 2020). The pervasive specter of ASFV engenders widespread and contagious outbreaks, significantly impacting the swine industry with profound economic consequences across Europe, the Caribbean, and Asia (Borca et al., 2020). Recent instances of ASFV, particularly in China, underscore its escalating global threat, eliciting substantial economic repercussions exceeding $130 billion, given China's pivotal role as the foremost global pig producer (Qu et al., 2022; Tran et al., 2022a; Wu et al., 2020). Despite assiduous research endeavors, the formulation of a potent vaccine or treatment for ASFV remains an enduring challenge, underscoring the imperative for efficacious therapeutic interventions (Urbano and Ferreira, 2022). Notably, recent studies reveal that ASFV induces significant spatio-temporal nuclear rearrangements, including ATR pathway activation and disruption of PML-NBs, which likely contribute to controlling host gene expression, favoring viral replication, and provide valuable insights for developing antiviral compounds and

* Corresponding author.
E-mail address: emersontseng@dragon.nchu.edu.tw (T.-S. Tseng).
[1] Equal contribution.

https://doi.org/10.1016/j.virusres.2024.199359
Received 15 January 2024; Received in revised form 15 March 2024; Accepted 17 March 2024

vaccines against ASFV (Simoes et al., 2013, 2015a, 2015b).

ASFV, part of the Asfarviridae family and Asfivirus genus, causes a severe hemorrhagic viral disease in domestic pigs and wild boars, often leading to nearly 100 % mortality for virulent strains (Galindo and Alonso, 2017; Li et al., 2022; Wang et al., 2019). This intricate, enveloped, double-stranded DNA virus has a genomic size of 170–190 kb, encoding at least 150 proteins crucial for biological processes (Wang et al., 2021c; Yanez et al., 1995). The linear DNA genome includes 151 to 167 open reading frames, with 24 distinct genotypes based on the major capsid protein p72 gene (Alejo et al., 2018; Sanchez-Cordon et al., 2018; Wang et al., 2021a). ASFV targets swine macrophages and monocytes, initiating DNA synthesis in the host nucleus, and undergoes replication in the cytoplasm, risking genome damage (Akaike, 2001; Alcami et al., 1990; Dixon et al., 2013; Forman and Torres, 2001). As global ASFV prevalence rises, effective prevention and control strategies are crucial. Progress in vaccine development, notably with ASFV-G-ΔI177L, requires ongoing scrutiny, especially for cross-protective potential (Borca et al., 2021b; Lopez et al., 2020; Monteagudo et al., 2017; O'Donnell et al., 2016; Ramirez-Medina et al., 2022; Sang et al., 2020; Tran et al., 2022a, 2022b; Wang et al., 2021b). Vaccine development faces challenges, including limited cell line availability, prompting exploration of DNA vaccines, vectored vaccines, and live attenuated vaccines with defined gene deletions (Borca et al., 2021a; Wang et al., 2021b). Despite promising in vitro results, safety concerns restrict live-attenuated vaccine implementation. Studies aim to identify compounds inhibiting ASFV, classifying antiviral drugs into nucleoside analogs, interferons, planD-1derived compounds, antibiotics, small interfering RNA, and CRISPR/Cas9 (Arabyan et al., 2018; Freitas et al., 2016; Galindo et al., 2011; Gil-Fernandez et al., 1979; Hakobyan et al., 2016, 2018; Hernaez et al., 2010; Keita et al., 2010; Paez et al., 1990; Zhu et al., 2020). Some antiviral drugs, like resveratrol, and apigenin show potent dose-dependent anti-ASFV activity in vitro, yet their specific targets and mechanisms remain undisclosed. Currently, no effective drugs for ASFV clinical trials are identified, emphasizing the urgent need for preventive and therapeutic agents.

ASFV replication predominantly occurs within the cytoplasm of swine macrophages, a primary source of continuous reactive oxygen species causing ongoing damage to the viral genome (Akaike, 2001; Alcami et al., 1990; Chen et al., 2020; Forman and Torres, 2001). The virus responds to potential DNA damage by activating its DNA repair apparatus, consisting of AP endonuclease (*Asfv*AP), repair DNA polymerase (*Asfv*PolX), and DNA ligase (*Asfv*LIG), triggered by the presence of apurinic/apyrimidinic (AP) sites or single-strand breaks (Lamarche et al., 2005; Lamarche and Tsai, 2006; Oliveros et al., 1997). *Asfv*PolX, working in tandem with *Asfv*LIG, significantly contributes to strategic mutagenesis and genotype formation in ASFV. Extensive scrutiny has focused on ASFV repair enzymes due to their functional significance (Garcia-Escudero et al., 2003; Redrejo-Rodriguez et al., 2006). *Asfv*PolX assumes a crucial role in the DNA repair mechanism of the ASFV genome, playing a pivotal role in viral replication efficiency. Its distinctive structural features, encompassing the 5′-phosphate binding pocket, a His115-Arg127 platform, and hydrophobic residues Val120 and Leu123, present specific sites for targeted inhibition. Conceivably, inhibiting this 5′-phosphate binding pocket through therapeutic means may disrupt *Asfv*PolX activity, consequently hampering the essential DNA repair process crucial for the viral genome (Chen et al., 2017). The 5′-phosphate binding pocket, serving as an optimal structural foundation, opens avenues for developing small molecules selectively targeting *Asfv*PolX, potentially offering therapeutic interventions. Thus, designing inhibitors to interact with these features allows selective impediment of *Asfv*PolX activity. This inhibition disrupts the DNA repair process within the ASFV genome, compromising genome integrity. Given the partial reliance of viral replication efficiency on proper *Asfv*PolX functioning, inhibiting this enzyme emerges as a viable strategy for disrupting the replication process and, consequently, controlling ASFV infections.

Computer-aided drug design (CADD) is a cosD-1effective and efficient method that accelerates the screening of inhibitors with specific biological activity (Kapetanovic, 2008). It encompasses both structure-based drug design (SBDD) and ligand-based drug design (LBDD) methods. Mostly, the scientific community has predominantly favored SBDD due to the widespread availability of crystallographic structures for diverse biological targets (Dos Santos Nascimento et al., 2022a, 2022b; Lin, 2022). SBDD, relying on 3D structures for various targets, is more commonly used, while LBDD encounters limitations in the absence of structural information about the target (Dos Santos Nascimento et al., 2022a, 2022b). Also, SBDD involves two main methods: pharmacophore modelling and molecular docking (Yu and MacKerell, 2017). The virtual high-throughput screening, using molecular docking, evaluates potential biological activities based on structural properties (Zoete et al., 2009). To efficiently identify potent inhibitors, it is crucial to consider functionally essential features for protein-ligand interactions. Pharmacophore modelling can be used to define the arrangement of essential ligand features for specific and effective binding to a receptor (Lu et al., 2018; Yang, 2010). The receptor-ligand pharmacophore generation (structure-based pharmacophores, SBPs) converts protein properties into reciprocal ligand space, allowing the design of ligands with desired properties for effective binding to a specific protein (Pirhadi et al., 2013). Several investigations have provided evidence for the effectiveness of SBPs in diverse applications (Behzadipour et al., 2021; Halim et al., 2017; Luo et al., 2021; Sun et al., 2011; Tsai et al., 2019, 2022; Tseng et al., 2016; Tung et al., 2021a, 2021b; Valasani et al., 2014; Zhou et al., 2019). The use of SBPs in virtual high-throughput screening is adept at efficiently identifying potential ligands with a high binding affinity to a specific protein, thereby expediting the drug discovery process. Notably, pharmacophore-based inhibitor screening demonstrates significant power in screening novel compounds that satisfy pharmacophore requirements and exhibit potential biological activity (Gao et al., 2010; Guner, 2005; Khedkar et al., 2007; Lu et al., 2018; Yang, 2010).

The current availability of the *Asfv*PolX-DNA complex's complex structure (PDB ID: 5HRB) facilitates the application of CADD for the screening and development of potent inhibitors. In this study, we conducted pharmacophore-based inhibitor screening, complemented by biochemical and biophysical examinations, leveraging the structure of the *Asfv*PolX-DNA complex to scrutinize, characterize, and validate potential inhibitors. Utilizing receptor-ligand pharmacophore generation, we systematically explored the functionally essential features of DNA interaction with *Asfv*PolX. The constructed pharmacophore model, **Phar-PolX-S**, encompassed bioactive features of DNA, enabling ligand-pharmacophore mapping for the screening of potential inhibitors. Consequently, among 68,285 compounds from the IBS database, five were identified with 50 % inhibitions against the formation of the *Asfv*PolX-DNA complex at a 100 μM compound concentration. Further inhibition assays demonstrated that **D-132** ($IC_{50} = 2.8 \pm 0.2$ μM), **D-166** ($IC_{50} = 4.5 \pm 0.3$ μM), and **D-609** ($IC_{50} = 9.3 \pm 0.5$ μM) displayed dose-dependent inhibitions, disrupting *Asfv*PolX-DNA complex formation. Moreover, localized surface plasmon resonance (LSPR) investigations disclosed that **D-132** bound to *Asfv*PolX with a binding affinity of 6.9 ± 2.2 μM. Additionally, the mode of action of **D-132** on *Asfv*PolX was investigated and revealed through structural analyses and molecular modelling. Our integrated approach, combining CADD with biochemical and biophysical techniques, successfully identified, characterized, and validated the inhibitor **D-132**, specifically targeting *Asfv*PolX. **D-132**, as an identified inhibitor, holds promise as a lead for further optimization into therapeutic agents to combat ASFV.

2. Material and methods

2.1. Preparations of the recombinant AsfvPolX protein

The construction of the *Asfv*PolX plasmid involved the integration of a synthetic His-SUMO-TEVsite-*Asfv*PolX gene into the pET28a vector by

CloneEZ seamless cloning. The synthesis and cloning of the gene into the pertinent expression vectors were conducted by Yao-Hong Biotechnology Inc. (http://www.yh-bio.com.tw/en/index.asp). Subsequently, the His-SUMO-TEVsite-*Asfv*PolX plasmid was introduced into *E. coli* Rosetta (DE3) pLysS, and bacterial cultivation occurred in LB medium at 37 ℃ with 50 mg/L kanamycin. Induction was initiated by treating the culture with 1.0 mM IPTG when the cell density reached $OD_{600} = 0.6$, and the incubation continued at 37 °C for 4 h. The cultured cells were harvested through centrifugation (6000 rpm for 20 min), resuspended in lysis buffer (20 mM Tris-HCl and 150 mM NaCl, pH 8.0), and subjected to disruption via a microfluidizer (Microfluidics). The resulting crude extract's supernatant underwent purification using nickel-nitrilotriacetic acid affinity resins (Qiagen, Hilden, Germany). The preliminarily purified His-SUMO-TEVsite-*Asfv*PolX protein was subjected to the digestion of TEV protease (molar ration = 1 : 0.15) incubating at 16 °C overnight to remove the SUMO fusion tag. The digested solution was further purified through the fast protein liquid chromatography (FPLC) using a Hitrap Capto S column. Finally, the purity of the sample was assessed using Coomassie blue-stained SDS polyacrylamide gel.

2.2. Preparations of DNA fragments

The double stranded oligonucleotides: 5′-CGGATATCC-3′ and 3′-CCTATAGGC-5′ (Chen et al., 2017) were synthesized and purchased from Yao-Hong Biotechnology Inc. The annealing of the double-stranded DNA (dsDNA) involved combining equal aliquots of two oligomers in a solution containing 20 mM sodium phosphate buffer and 150 mM NaCl at pH 6.0. This mixture was subjected to heating at 95 °C followed by a gradual cooling to room temperature. Following the annealing process, ion exchange chromatography, employing a Mono-Q 5/50 GL column (Amersham Biosciences), was utilized for the purification of the annealed dsDNA products.

2.3. Analysis of DNA binding property of AsfvPolX by fluorescence polarization assay

The oligonucleotide (5′-CGGATATCC-3′) designated for the fluorescence polarization experiment was labeled with 6-carboxyfluorescein (6-FAM) at the 5′ position. The *Asfv*PolX protein, at varying concentration of interest, was introduced into wells containing 10 nM of 6-FAM-labeled DNA in a reaction buffer consisting of 20 mM sodium phosphate and 150 mM NaCl at pH 6.0, maintained at 25 °C. Measurements of the reactions were conducted three times using the Synergy H1MF plate reader (BioTek Instruments, Inc.) with an excitation wavelength of 485 nm and an emission wavelength of 535 nm. Subsequently, binding curves were fitted using one- or two-binding models, and data were analyzed and plotted using GraphPad Prism 6 (San Diego, CA, USA).

2.4. Ligands preparations for computer-aided inhibitor screening

A total of 68,285 compounds sourced from InterBioScreen (IBS, http://www.ibscreen.com) was obtained for computer-aided inhibitor screening. The molecular structures of all compounds were generated using the sketch molecules and prepare ligands modules of Discovery Studio 2021 (Accelrys Software, Inc., San Diego, CA, USA). The compounds selected for ligand-pharmacophore mapping and molecular docking analyses underwent a three-step preparation process: (1) conversion of 2D structures to 3D structures, (2) calculation of molecular charges, and (3) addition of hydrogen atoms. Subsequently, receptor-ligand pharmacophore generation and pharmacophore-based inhibitor screening (ligand-pharmacophore mapping) were conducted.

2.5. Receptor-ligand pharmacophore generation and ligand-pharmacophore mapping

Pharmacophore modeling of receptor-ligand interactions offers precision in identifying crucial features essential for ligands to engage with target proteins. In this study, we utilized the *Asfv*PolX-DNA complex structure (PDB ID: 5HRB) to construct a pharmacophore model, encompassing interactive features, for the purpose of screening potential inhibitors. The receptor-ligand pharmacophore generation module of Discovery Studio 2021 was employed for this task. The *Asfv*PolX structure served as the "Input Receptor," while the DNA structure was used as the "Input Ligand". The parameters for pharmacophore generation were set as follows: "Minimum Features" and "Maximum Features" were established at 10 and 30, respectively, and the "Maximum Pharmacophores" was set to 10. The "fast method" was applied for conformation generation using the "rigid fitting method," and the remaining parameters were maintained at their default settings. Subsequently, the constructed pharmacophore model underwent ligand-pharmacophore mapping. For the mapping process, all molecules from the IBS database (https://www.ibscreen.com/) (comprising 68,285 compounds) were fitted to the generated pharmacophore model. The fitting method employed was "flexible," with all other parameters kept at their default settings.

2.6. The inhibitory activities of compounds determined by fluorescence polarization (FP) measurements

The oligonucleotide (5′-CGGATATCC-3′) obtained from the determined *Asfv*PolX-DNA complex (Chen et al., 2017), labeled with 6-FAM at the 5′ position, was dissolved in a solution of 20 mM sodium phosphate and 150 mM NaCl at pH 6.0 for fluorescence polarization experiments. For each experiment, approximately 10 μl of *Asfv*PolX, prepared in a buffer of 20 mM sodium phosphate and 150 mM NaCl at pH 6.0, was initially added to an ELISA plate well. Following this, 1 μl of serially diluted inhibitors were mixed with the *Asfv*PolX (final concentration 1.0 μM) to achieve the desired concentrations. The mixture was then incubated at 25 °C for 10 min. Subsequently, 9 μl of 6-FAM-labeled DNA (final concentration = 10 nM) was added to the reaction, and the incubation continued at 25 °C for another 10 min. The reactions were measured three times using a Synergy H1MF plate reader (BioTek Instruments, Inc) with an excitation wavelength of 485 nm and an emission wavelength of 535 nm. The inhibition percentage was calculated using the following equation:

$$Inhibition\ \% = \frac{\{[(P+D)-(D)]-[(P+I+D)-(D)]\}}{[(P+D)-(D)]} \times 100$$

where (D), $(P + D)$, and $(P + I + D)$ denote the polarization intensity of DNA alone, PhoP bound with DNA, and PhoP mixed with inhibitor and then incubated with DNA, respectively.

2.7. Localized surface plasmon resonance

The binding affinity of the identified inhibitors to *Asfv*PolX was determined and analyzed using an OpenSPR instrument (Nicoya Lifesciences Inc.). The *Asfv*PolX protein solution was prepared in 1X PBS buffer at pH 7.3. Immobilization of the *Asfv*PolX protein (80 μg/ml) onto an NTA sensor chip was performed, and the interaction with fluid-phase inhibitors was subsequently detected. The inhibitors (analytes) were prepared in 1X PBS buffer containing 0.5 % DMSO and 2 % BSA at various concentrations for detection. Throughout the analysis, the chip was regenerated using a 10 mM glycine-HCl buffer at pH 2.2 for each experiment. The obtained data were fitted to a 1:1 binding model using Trace Drawer software to determine the KD (dissociation constant) value.

2.8. Preparation of protein structure for LibDock docking

Before conducting the LibDock molecular docking, the protein structure of *Asfv*PolX (PDB ID: 5HRB) underwent meticulous

preparation. Initially, the residues of *Asfv*PolX involved in interactions with DNA were utilized to define the binding site. Following this, the site sphere was constructed based on the selection, and the DNA was subsequently removed from the active site of *Asfv*PolX. The processed *Asfv*PolX structure was further refined using the "prepare protein" function in Discovery Studio 2021, involving the following steps: (i) Standardization of atom names, insertion of missing atoms in residues, and removal of alternate conformations. (ii) Insertion of missing loop regions based on either SEQRES data or user-specified loop definitions. (iii) Optimization of short and medium-sized loop regions using the LOOPER algorithm. (iv) Minimization of the remaining loop regions. (v) Calculation of pK and protonation of the structure. All remaining parameters were set to default values to prepare the protein structure of *Asfv*PolX for LibDock molecular docking.

2.9. Construction of the complex structure of AsfvPolX-inhibitors by LibDock molecular docking

Structure-based molecular docking analysis was conducted using LibDock, implemented in Discovery Studio 2021, to generate the complex structure of *Asfv*PolX-inhibitor. In this process, the protein structure of PolX (PDB ID: 5HRB) was employed to define and edit the docking site. The residues of *Asfv*PolX involved in interactions with DNA were utilized to define the binding site for subsequent protein-ligand docking, and the protein structure of *Asfv*PolX was prepared according to the steps described in the preparation of the protein structure for LibDock docking. Subsequently, the site sphere was constructed based on the selection and utilized for LibDock screening. The structure of *Asfv*PolX was served as the "Input Receptor," while the identified inhibitor was used "Input Ligands." The identified inhibitor, **D-132**, was docked into the active site of *Asfv*PolX with "High Quality" set for the "Docking Preferences" and "BEST" selected for the "Conformation Method." The "Number of Hotspots" was configured as "100," and the "Docking Tolerance" was set to "0.25." Additionally, the "Smart Minimizer" was employed as the "Minimization Algorithm," while the remaining parameters were kept as default. Following the calculations, the orientations and positions with the highest LibDockScore were chosen, examined, and analyzed using ligplot (Laskowski and Swindells, 2011; Wallace et al., 1995).

3. Results

3.1. Receptor-ligand pharmacophore generation

In this study, we adopted an integrated approach involving computer-aided drug design (CADD), alongside biochemical and biophysical analyses, to identify, characterize, and validate potential inhibitors targeting *Asfv*PolX. The application of receptor-ligand pharmacophore modeling enabled the exploration of crucial functional features governing the interactions between DNA and *Asfv*PolX. Given the pivotal role of structural information from the *Asfv*PolX-DNA complex, we utilized the complex structure (PDB ID: 5HRB) (Fig. 1A) for constructing the pharmacophore model through receptor-ligand pharmacophore generation. During this construction, the *Asfv*PolX moiety functioned as the receptor, while the DNA structure served as the ligand for building the pharmacophore model, encapsulating functionally important features crucial for inhibitor screening. The resultant pharmacophore model, designated **Phar-PolX**, exhibited clustered features, as depicted in Fig. 1B. **Phar-PolX** encompasses 12 hydrogen-bond acceptors (green spheres), 1 ring aromatic (orange spheres), 2 hydrophobic aromatic features (cyan spheres), and 4 negatively charged features (blue spheres) (Fig. 1B). This pharmacophore model provides a comprehensive representation of the critical molecular features essential for potential inhibitor binding.

3.2. Pharmacophore-based inhibitor screening

Efficient inhibitor screening through pharmacophore modeling relies significantly on the judicious selection of a pharmacophore scaffold for ligand-pharmacophore mapping. In this regard, we conducted a comprehensive exploration of the pharmacophore features within **Phar-PolX**. Our findings revealed that 1 aromatic ring (Aro1), 2 negatively charged features (N1 and N2), and 1 hydrogen-bond acceptor (HA1) collectively constitute a bioactive scaffold representing the DNA interaction with residues G38, R42, N48, Q98, H115, F116, and V120 (Fig. 2A). These features of **Phar-PolX** were subsequently grouped as a pharmacophore scaffold, **Phar-PolX-S** (Fig. 2B), and utilized for the screening of potential inhibitors. A compound library comprising 68,285 molecules was sourced from the IBS database, and ligand-pharmacophore mapping was executed to fit these compounds onto **Phar-PolX-S**. In this mapping process, the 3D coordinates of the ligands were aligned with the pharmacophore features of **Phar-PolX-S**, and the fit between the ligand and the pharmacophore was evaluated. The fit values served as indicators of the quality of the match between the ligand and the pharmacophore, with higher scores indicative of a better fit. Consequently, the top 10 ranked hits were selected as potential candidates (Fig. 3). The hierarchy of the fit values is as follows: **D-053** > **D-270** > **D-093** > **D-582** > **D-439** > **D-142** > **D-132** > **D-166** > **D-609** > **D-884**. The detailed chemical structures of these identified hits are presented in Table S1.

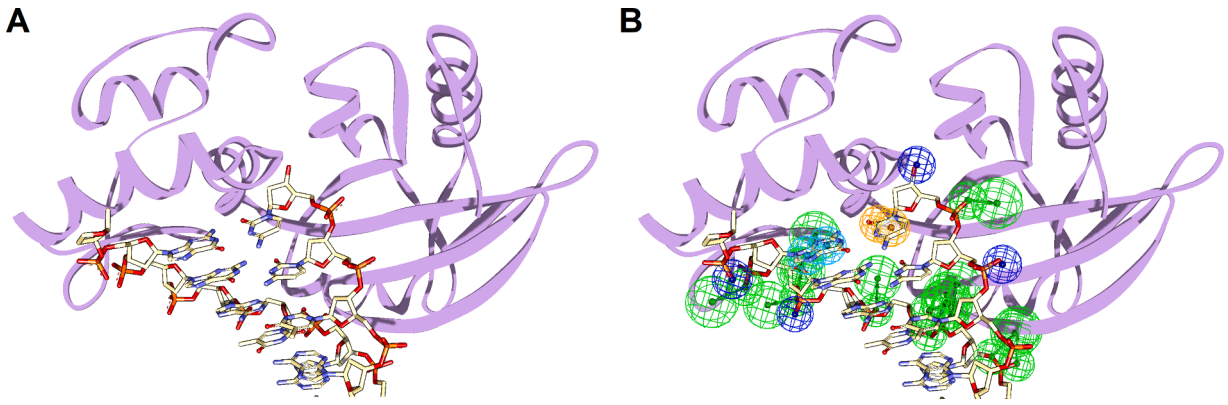

Fig. 1. The receptor-ligand pharmacophore generation based on the structure of *Asfv*PolX-DNA complex. (A) The complex structure of *Asfv*PolX-DNA (PDB ID: 5HRB) was used to build the pharmacophore models. The protein structure is shown in ribbons and the DNA molecule is presented in sticks. **(B)** The generated pharmacophore features are shown along with the structure of *Asfv*PolX-DNA complex. The pharmacophore features are color-coded as follows: green, hydrogen bond acceptor; cyan, hydrophobic; orange, ring aromatic; deep-blue, negative charged features.

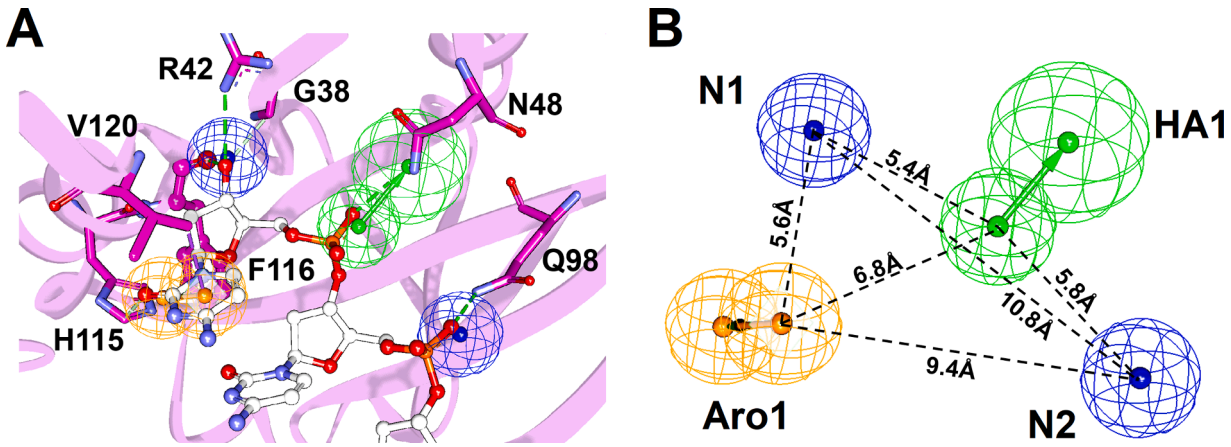

Fig. 2. Schematic representations of pharmacophore model, Phar-PolX-S. (A) The pharmacophore scaffold of **Phar-PR-S** aligned with the structure of DNA (white sticks); the interactive residues of *Asfv*PolX are shown in magenta sticks and labelled. **(B)** Features at a specific distance correspond to the pharmacophore model, **Phar-PolX-S**. (Pharmacophore features are colored as follows: green, hydrogen bond acceptor; cyan, hydrophobic; orange, ring aromatic; deep-blue, negative charged features.)

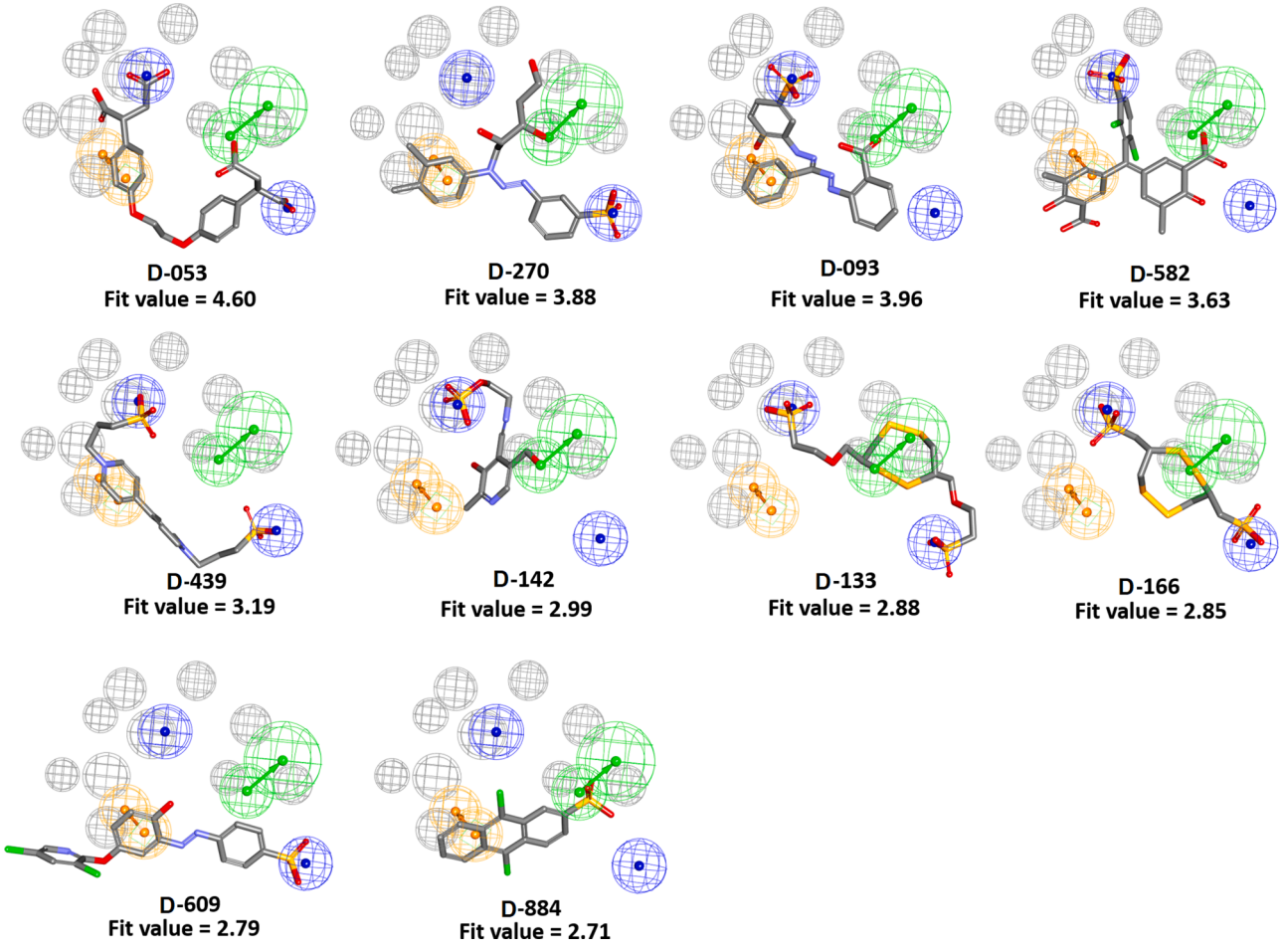

Fig. 3. Pharmacophore-based inhibitor screening. The results of ligand pharmacophore (**Phar-PolX-S**) mapping of hits screened from IBS database. The top10 ranked hits are fitted with pharmacophore model, **Phar-PolX-S**. (Pharmacophore features are colored as follows: green, hydrogen bond acceptor; cyan, hydrophobic; orange, ring aromatic; deep-blue, negative charged features. The gray spheres indicate the excluded volumes.)

3.3. The disruptive ability of inhibitors against the formation of PolX-DNA complex

To further assess the inhibitory potential of the identified hits against *Asfv*PolX binding to DNA, fluorescence polarization (FP) experiments were conducted. Prior to this, the DNA binding property of *Asfv*PolX was initially characterized to establish the assay platform for inhibition. The *Asfv*PolX was successfully expressed and purified (Figure S1). The DNA sequence (5′-CGGATATCC-3′) was employed for the FP experiment to measure the DNA binding affinity of *Asfv*PolX. The results indicated an

increase in polarization intensity with ascending concentrations of *Asfv*PolX protein (Fig. 4). This demonstrated a strong binding affinity of *Asfv*PolX to DNA, with a KD value of 0.01 μM. Notably, the polarization intensity reached a plateau when the concentration of *Asfv*PolX exceeded 1.0 μM. Consequently, 1.0 μM of *Asfv*PolX was selected for subsequent inhibition assays. Furthermore, the inhibitory capabilities of the top 10 hits identified from the pharmacophore-based inhibitor screening were evaluated at a compound concentration of 100 μM. The results revealed that compounds **D-132, D-166, D-609, D-582**, and **D-093** exhibited over 50 % inhibitions, as shown in Fig. 5. Conversely, **D-142, D-884, D-439, D-053**, and **D-270** showed less or no inhibition against *Asfv*PolX binding to DNA (Fig. 5). Subsequently, hits with over 50 % inhibitions were subjected to inhibitory experiments at various compound concentrations to determine their IC_{50} values. In the inhibition of *Asfv*PolX binding to DNA, **D-132, D-166, D-609, D-093**, and **D-582** demonstrated dose-dependent inhibitions, with determined IC_{50} values of 2.8 ± 0.2, 4.5 ± 0.3, 9.3 ± 0.5, 25.1 ± 1.3, and 35.2 ± 1.8 μM, respectively (Fig. 6).

3.4. The binding affinities of D-132 and D-166 towards AsfvPolX

In our pharmacophore-based inhibitor screening, we identified that **D-132** and **D-166** were two strong inhibitors against *Asfv*PolX. To further confirm the interactions of inhibitors to *Asfv*PolX, their binding affinities were investigated by using localized surface plasmon resonance (LSPR). During the LSPR experiments, inhibitor **D-132** was tested at 6.25, 12.5, 25, and 50 μM. The sensorgrams showed slow association and fast dissociation binding manner of **D-132** to *Asfv*PolX, resulting a KD value of 6.92 ± 2.2 μM (Fig. 7A). In addition, the binding of **D-166** to *Asfv*PolX was investigated at 12.5, 50, 100 and 300 μM. The result demonstrated that **D-166** employed a slow association and slow dissociation manner to bind with *Asfv*PolX (Fig. 7B).

3.5. The complex structure of AsfvPolX-D-132

To attain a more comprehensive understanding of the atomic-level interactions between *Asfv*PolX and the identified inhibitor **D-132**, molecular modeling techniques were employed to construct the complex structure. The residues of *Asfv*PolX involved in interactions with DNA were utilized to define the binding site for subsequent protein-ligand docking. Following the docking simulation, **D-132** closely conformed to the characteristics of **Phar-PolX-S**, was selected as the final complex

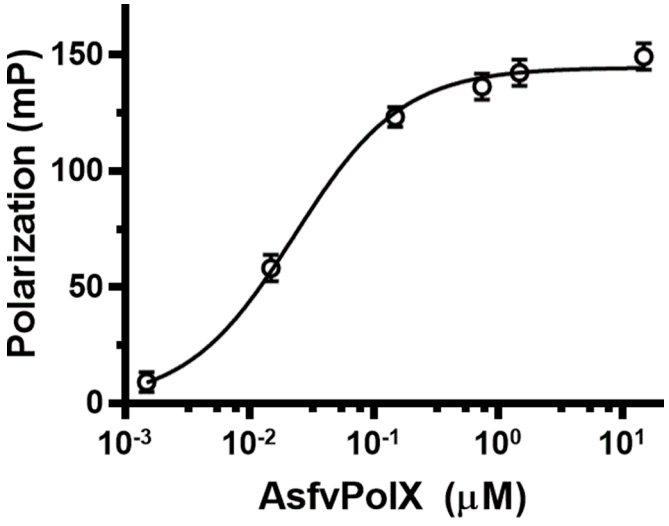

Fig. 4. The DNA binding property of *Asfv*PolX. (A) The DNA binding ability of *Asfv*PolX is observed by FP experiments as a function of protein concentration. The determined KD value is 0.01 μM.

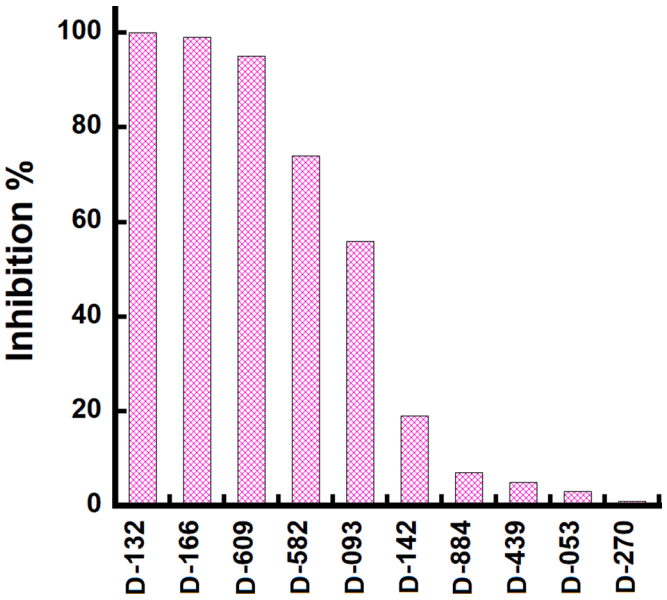

Fig. 5. The inhibitory potency of top10 ranked hits against *Asfv*PolX binding to DNA binding. The inhibitory ability of top10 ranked hits against the formation of *Asfv*PolX-DNA complex was determined at 100 μM and shown.

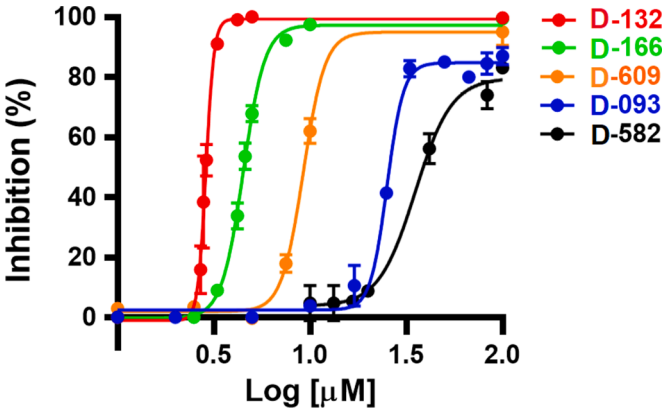

Fig. 6. The potencies of identified inhibitors as a function of compound concentration. Compounds, **D-132, D-166, D-609, D-093**, and **D-582** exert dose-dependent inhibition against the formation of *Asfv*PolX-DNA.

structure. This constructed complex structure was further subjected to non-bond interaction analysis (Discovery Studio 2021) to unveil detailed molecular interactions. The specific molecular interactions between **D-132** and *Asfv*PolX were visualized in Fig. 8. Notably, in this binding orientation, the terminal sulfonic groups of **D-132**, corresponding to N1 and N2 of **Phar-PolX-S**, engaged in charge-charge interactions with residues R42 and Q98. Remarkably, residue N48 formed hydrogen bond interactions with **D-132**. Additionally, the S2 and S3 atoms on the 1,2,5,6-tetrathiocane moiety of **D-132** formed pi-sulfur interactions with the side chain of residue F116. Furthermore, residue F102 interacted with the 1,2,5,6-tetrathiocane moiety of **D-132** through a hydrophobic interaction (Fig. 8A and C). Besides, residue E100 demonstrated interactions with **D-132** through a carbon-hydrogen bond.

4. Discussion

African swine fever virus (ASFV) poses a severe threat to global swine populations due to its highly contagious and lethal nature. Its geographical spread beyond Africa, with recent outbreaks in Asia,

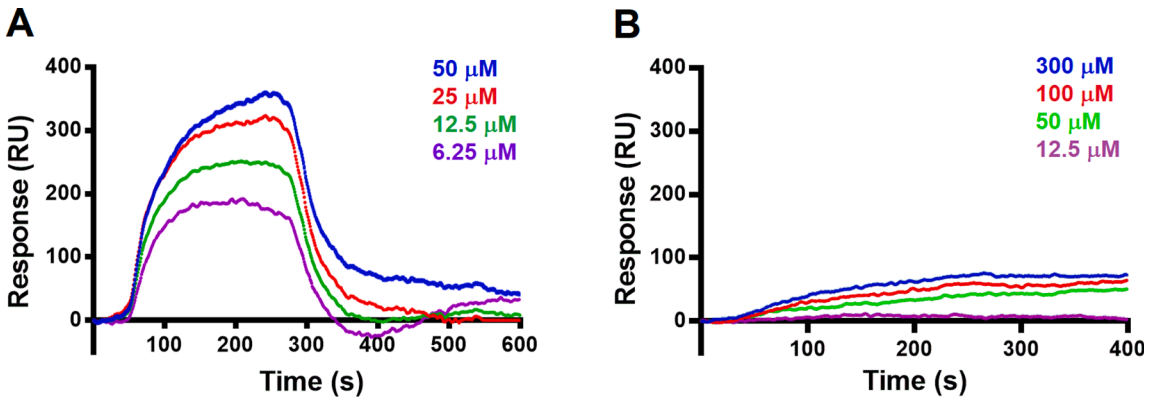

Fig. 7. The SPR sensorgrams of D-132 and D-166 binding to *Asfv*PolX. (A) The binding affinity of **D-132** (KD = 6.9 ± 2.2 μM) to *Asfv*PolX. **(B)** The binding responses of **D-166** to *Asfv*PolX.

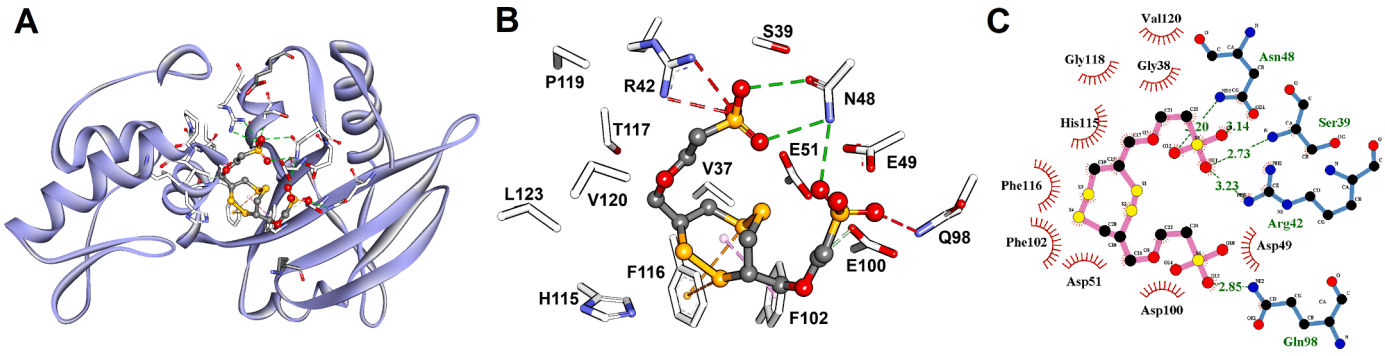

Fig. 8. The modelled complex structure and molecular interactions of *Asfv*PolX-D-132. (**A**) The complex structure of *Asfv*PolX-**D-132** was built by molecular docking. The *Asfv*PolX and **D-132** are shown in ribbon and ball-and-stick, respectively. (**B**) The amplified view of **D-132** binds in the DNA binding site of *Asfv*PolX. The dash lines colored in green, orange, light-pink, light-green, and red denote the hydrogen bonding, pi-sulfur interaction, hydrophobic interaction, carbon hydrogen bond, and charge-charge interaction, respectively. (**C**) The detailed molecular interactions of **D-132** binding to *Asfv*PolX is shown in 2D schematic plot analyzed by ligplot.

exacerbates economic challenges in the swine industry. The primary tools for preventing and controlling viral infections are vaccines and antiviral drugs (Monto, 2006). Despite extensive efforts, encompassing the creation of vaccines such as ASFV-G-ΔI177L and the investigation of antiviral compounds, conclusive preventive or therapeutic resolutions for ASFVs have remained elusive (Sanchez et al., 2019). Brincidofovir, known for its broad-spectrum antiviral activity against double-stranded DNA viruses, emerges as a potential candidate against ASFV (Guo et al., 2023). However, further research and clinical trials are imperative to evaluate its effectiveness in mitigating ASFV infections. Given the absence of vaccines against ASFV, the utilization of antiviral drugs becomes imperative, not only for enhancing host survival but also for contributing to epidemic control (Zakaryan and Revilla, 2016). This underscores the pressing necessity to develop effective antiviral interventions against ASFVs, addressing the current challenges in ASFV control.

Various compounds demonstrating inhibitory potential against ASFV infections have been identified in diverse studies, categorizable into two groups (Arabyan et al., 2019). The first group comprises antiviral drugs with specific targets and mechanisms, including nucleoside analogs like iododeoxyuridine (Gil-Fernandez et al., 1979). Additionally, planD-1derived compounds, such as genistein (Arabyan et al., 2018) and genkwanin (Hakobyan et al., 2019), hinder viral type II topoisomerase and impede virus movement along microtubules, respectively. SiRNAs and CRISPR/Cas9, specifically targeting viral genes A151R and B646L (Keita et al., 2010), demonstrate substantial reductions in virus titer and RNA transcripts. Furthermore, interferons (IFNs) like IFN-alpha (Paez et al., 1990) and IFN-gamma (Hicks et al., 1981), can disrupt the interaction between cytoplasmic dynein and viral p54 protein (Hernaez et al., 2010). Antibiotics, including Rifampicin (Dardiri et al., 1971) and fluoroquinolone (Mottola et al., 2013), hinder viral DNA-dependent RNA polymerase and type II topoisomerases. The second category of antiviral drugs, represented by Apigenin (Hakobyan et al., 2016), resveratrol (Galindo et al., 2011), and oxyresveratrol (Galindo et al., 2011), features unknown targets and mechanisms. However, none of the mentioned antiviral drugs have progressed to commercial production, emphasizing the ongoing need for novel candidate drugs. Recent emphasis on ASFV inhibitors revolves around *Asfv*PolX, a key player in viral DNA repair. Its unique structural features, particularly the 5′-phosphate binding pocket, provide a foundation for developing antiviral compounds. The global urgency for effective ASFV control has driven research into inhibiting *Asfv*PolX, with a focus on its distinctive structural features, notably the 5′-phosphate binding pocket, showing promise for precise antiviral compound development. Comprehensive studies and clinical investigations are imperative for translating these findings into practical solutions for combating ASFV. Therefore, in this study, we aimed to develop potent inhibitors targeting *Asfv*PolX, utilizing computer-aided drug design (CADD) coupled with biochemical and biophysical examinations to screen, characterize, and validate inhibitors against *Asfv*PolX, offering a potential solution for ASFV management.

Computational approaches such as Computer-Aided Drug Design (CADD), involving molecular docking and pharmacophore modeling, offer a cosD-1effective means for the systematic screening of compounds with specific biological functionalities. Pharmacophore modeling, particularly the generation of structure-based pharmacophores (SBPs) or

receptor-ligand pharmacophores, facilitates the translation of protein properties into corresponding ligand features. This approach is instrumental in the development of inhibitors with precisely defined characteristics for effective binding to the target protein. Therefore, the availability of structural insights from the *Asfv*PolX-DNA complex plays a crucial role in the identification of potential inhibitors.

Notably, Chen *et al.* successfully determined eight crystal structures, encompassing four *Asfv*PolX-DNA binary complexes and four *Asfv*PolX-DNA-dGTP ternary complex structures, representing distinct reaction states—prior to dNTP incorporation and after dNTP incorporation (Chen et al., 2017). Additionally, the superposition analysis of the eight complex structures revealed a shared DNA-interacting site common to all DNA molecules. This binding site, primarily composed of residues from two regions ($_{81}$CGERK$_{85}$ from the palm domain and $_{135}$YKLNQY$_{140}$ from the finger domain), formed extensive interactions with the DNA template strand. Therefore, in this study, we utilized the complex structures of *Asfv*PolX-DNA (PDB ID: 5HRB) to comprehensive explore the pharmacophore features within this common DNA-interacting site. Utilizing *Asfv*PolX as the receptor and DNA as the ligand, the pharmacophore model, **Phar-PolX**, was created, encompassing hydrogen-bond acceptors, negative-charged, hydrophobic, and ring aromatic features (Fig. 1B). These features collectively provide a comprehensive representation of the essential attributes required for ligand binding and interaction with the *Asfv*PolX-DNA complex, thereby facilitating the identification and design of potential inhibitors. Additionally, a DNA bioactive scaffold interacting with specific residues (G38, R42, N48, Q98, H115, F116, and V120 (Fig. 2)) was effectively represented by two negatively charged features (N1 and N2), one hydrogen-bond acceptor (HA1), and one ring aromatic feature (Fig. 2). These features served as the foundation for the creation of a pharmacophore scaffold termed **Phar-PolX-S**. Moreover, the top 10 ranked hits identified through ligand-pharmacophore (**Phar-PolX-S**) mapping exhibited varying degrees of inhibitory effects (Fig. 5). Subsequent dose-dependent inhibition assays demonstrated that **D-132** and **D-166** displayed robust inhibitory abilities against *Asfv*PolX-DNA complex formation, as validated by fluorescence polarization assays (IC_{50} = 2.8 ± 0.2 and 4.5 ± 0.3 μM) (Fig. 6). These findings underscore the reliability and precision of the pharmacophore model, **Phar-PolX-S**, in screening inhibitors against *Asfv*PolX-DNA complex formation. Furthermore, the identified compounds, **D-132** and **D-166**, featuring sulfate groups at both termini, may mimic the functional phosphate groups of DNAs, engaging in electrostatic interactions with *Asfv*PolX.

Furthermore, the localized surface plasmon resonance (LSPR) experiments revealed distinct binding behaviors of **D-132** and **D-166** with *Asfv*PolX. **D-132** exhibited concentration-dependent binding, indicating a pronounced affinity with a KD value of 6.9 ± 2.2 μM (Fig. 7A). In contrast, **D-166** displayed weak binding signals, even at a higher concentration of 300 μM, suggesting limited affinity for *Asfv*PolX (Fig. 7B). The weak binding of **D-166** implies its ineffectiveness in interfering with the AsfvPolX-DNA interaction, while the evident binding affinity of **D-132** suggests its effective interaction with *Asfv*PolX. Further optimization and modification of **D-132** could enhance its potential in disrupting *Asfv*PolX-related processes. Additionally, for a comprehensive understanding of atomic interactions, molecular modeling was employed to construct the complex structure. The model with the lowest energy, closely resembling **Phar-PolX-S** characteristics, was selected as the final complex structure (Fig. 8). Non-bond interaction analysis unveiled that **D-132**, mirroring **Phar-PolX-S**, occupied the DNA binding site of *Asfv*PolX (Fig. 8). Noteworthy interactions included charge-charge interactions with R42 and Q98, carbon-hydrogen bonding with E100, hydrogen bonding with N84, pi-sulfur interaction with F116, and hydrophobic contacts with F102. These detailed molecular interactions elucidate the specific binding orientation and key residues involved, enhancing our comprehension of how **D-132** disrupts *Asfv*PolX function, potentially guiding the development of drugs targeting *Asfv*PolX for therapeutic applications.

Recently, Choi et al. employed molecular docking and machine learning techniques with DrugBank database to predict potential antiviral drugs against ASFV (Choi et al., 2021b). Their docking simulations were conducted on both apo-*Asfv*PolX and *Asfv*PolX-DNA complex structures, and molecules were compared based on eight molecular descriptors through principal component analysis. They found that pentagastrin exhibited 60 % inhibition of *Asfv*PolX activity at 100 μM concentrations in vitro. Additionally, utilizing the 5′-P binding pocket of *Asfv*PolX as a potential binding site, Choi et al. categorized 13 *Asfv*PolX structures into three classes based on SiteMap-calculated pocket parameters(Choi et al., 2021a) to identify antiviral drugs. They employed principal component analysis to mitigate scoring bias, resulting in a more balanced SP Glide score distribution among the 13 *Asfv*PolX structures. Consequently, they demonstrated that fostamatinib exhibited a dose-dependent decrease in *Asfv*PolX activity and was identified as potential antiviral drug against ASFV. In our study, **D-132** demonstrated a dose-dependent inhibitory effect, with an IC_{50} value of 2.8 ± 0.2 μM. In contrast, fostamatinib and pentagastrin, identified as potential antiviral drugs against ASFVs, but their specific IC_{50} values are not provided in Choi's approaches. To extend the comparison of inhibitory effectiveness, we executed an FP-based inhibition assay at a compound concentration of 100 μM. Strikingly, the inhibition against the formation of the *Asfv*PolX-DNA complex for **D-132**, fostamatinib and pentagastrin were determined as 100, 0, and 0 %, respectively (Figure S2. The observed results were not consistent with the finding of Choi *et al.* Indeed, our study demonstrated the binding affinity of **D-132** to *Asfv*PolX through LSPR experiments, revealing a KD value of 6.92 ± 2.2 μM. While specific IC_{50} values as well as the binding affinity for fostamatinib and pentagastrin towards *Asfv*PolX are not elucidated in Choi's research. Therefore, an in-depth exploration of factors such as their binding affinities, specificity, and mechanisms of action is essential for a nuanced understanding of the detailed functional distinctions of fostamatinib, and pentagastrin in impeding *Asfv*PolX binding to DNA.

5. Conclusion

In conclusion, our study employed a comprehensive approach encompassing computer-aided drug design, biochemical, and biophysical analyses to discern potential inhibitors targeting *Asfv*PolX. The generated receptor-ligand pharmacophore model (**Phar-PolX-S**) elucidated critical features governing inhibitor binding to the *Asfv*PolX-DNA complex. Through pharmacophore (**Phar-PolX-S**)-based screening, **D-132** emerged as a potent inhibitor, displaying the dose-dependent inhibitory effect and a discernible IC_{50} value (IC_{50} = 2.8 ± 0.2 μM). **D-132** exhibited strong binding to *Asfv*PolX (KD = 6.9 ± 2.2 μM) through a slow-on-fast-off binding mechanism. Subsequent molecular modeling of the *Asfv*PolX-**D-132** complex elucidated specific interactions, underscoring the strength of the binding affinity, and the interactive and functionally essential residues (R42, N48, Q98, E100, F102, and F116) act as hotspots for structure-based inhibitor optimization. Our study contributes valuable insights for the prospective development of inhibitor targeting *Asfv*PolX for combating ASFV infections.

Authorship statement

Every individual meeting the authorship criteria has been included as an author, and all authors confirm their substantial contribution to the work, encompassing involvement in conceptualization, design, analysis, writing, or revision of the manuscript. Additionally, each author affirms that the material, or similar content, has not been and will not be submitted to or published in any other publication prior to its appearance in Virus Research.

CRediT authorship contribution statement

Yi-Chen Wu: Validation, Methodology, Investigation, Data curation.

Hui-Xiang Lai: Validation, Methodology, Investigation, Data curation. **Ji-Min Li:** Validation, Methodology, Investigation, Data curation. **Kit-Man Fung:** Validation, Resources, Methodology, Data curation. **Tien-Sheng Tseng:** Writing – review & editing, Writing – original draft, Visualization, Validation, Supervision, Software, Resources, Project administration, Methodology, Investigation, Funding acquisition, Formal analysis, Data curation, Conceptualization.

Declaration of competing interest

The authors declare that they have no known competing financial interests or personal relationships that could have appeared to influence the work reported in this paper.

Data availability

Data will be made available on request.

Acknowledgements

We thank to National Center for High-performance Computing (NCHC) for providing computational and storage resources. This study was supported by the National Science and Technology Council, Taiwan (NSTC-111-2311-B-005-006- and NSTC 112-2320-B-005-010-MY3).

Supplementary materials

Supplementary material associated with this article can be found, in the online version, at doi:10.1016/j.virusres.2024.199359.

References

Akaike, T., 2001. Role of free radicals in viral pathogenesis and mutation. Rev. Med. Virol. 11 (2), 87–101.
Alcami, A., Carrascosa, A.L., Vinuela, E., 1990. Interaction of African swine fever virus with macrophages. Virus Res. 17 (2), 93–104.
Alejo, A., Matamoros, T., Guerra, M., Andres, G., 2018. A proteomic atlas of the African swine fever virus particle. J. Virol. 92 (23), e01293–18.
Arabyan, E., Hakobyan, A., Kotsinyan, A., Karalyan, Z., Arakelov, V., Arakelov, G., Nazaryan, K., Simonyan, A., Aroutiounian, R., Ferreira, F., Zakaryan, H., 2018. Genistein inhibits African swine fever virus replication in vitro by disrupting viral DNA synthesis. Antiviral Res. 156, 128–137.
Arabyan, E., Kotsynyan, A., Hakobyan, A., Zakaryan, H., 2019. Antiviral agents against African swine fever virus. Virus Res. 270, 197669.
Behzadipour, Y., Gholampour, M., Pirhadi, S., Seradj, H., Khoshneviszadeh, M., Hemmati, S., 2021. Viral 3CL(pro) as a target for antiviral intervention using milk-derived bioactive peptides. Int. J. Pept. Res. Ther. 27 (4), 2703–2716.
Borca, M.V., Rai, A., Ramirez-Medina, E., Silva, E., Velazquez-Salinas, L., Vuono, E., Pruitt, S., Espinoza, N., Gladue, D.P., 2021a. A cell culture-adapted vaccine virus against the current African swine fever virus pandemic strain. J. Virol. 95 (14), e0012321.
Borca, M.V., Ramirez-Medina, E., Silva, E., Vuono, E., Rai, A., Pruitt, S., Espinoza, N., Velazquez-Salinas, L., Gay, C.G., Gladue, D.P., 2021b. ASFV-G-ΔI177L as an effective oral nasal vaccine against the Eurasia strain of Africa swine fever. Viruses 13 (5).
Borca, M.V., Ramirez-Medina, E., Silva, E., Vuono, E., Rai, A., Pruitt, S., Holinka, L.G., Velazquez-Salinas, L., Zhu, J., Gladue, D.P., 2020. Development of a highly effective African swine fever virus vaccine by deletion of the I177L gene results in sterile immunity against the current epidemic Eurasia strain. J. Virol. 94 (7), e02017–19.
Chen, Y., Chen, X., Huang, Q., Shao, Z., Gao, Y., Li, Y., Yang, C., Liu, H., Li, J., Wang, Q., Ma, J., Zhang, Y.Z., Gu, Y., Gan, J., 2020. A unique DNA-binding mode of African swine fever virus AP endonuclease. Cell Discov. 6, 13.
Chen, Y., Zhang, J., Liu, H., Gao, Y., Li, X., Zheng, L., Cui, R., Yao, Q., Rong, L., Li, J., Huang, Z., Ma, J., Gan, J., 2017. Unique 5′-P recognition and basis for dG:dGTP misincorporation of ASFV DNA polymerase X. PLoS Biol. 15 (2), e1002599.
Choi, J., Tark, D., Lim, Y.S., Hwang, S.B., 2021a. Identification of African swine fever virus inhibitors through high performance virtual screening using machine learning. Int. J. Mol. Sci. 22 (24).
Choi, J., Yun, J.S., Song, H., Shin, Y.K., Kang, Y.H., Munashingha, P.R., Yoon, J., Kim, N. H., Kim, H.S., Yook, J.I., Tark, D., Lim, Y.S., Hwang, S.B., 2021b. Prediction of African swine fever virus inhibitors by molecular docking-driven machine learning models. Molecules 26 (12).
Costard, S., Mur, L., Lubroth, J., Sanchez-Vizcaino, J.M., Pfeiffer, D.U., 2013. Epidemiology of African swine fever virus. Virus Res. 173 (1), 191–197.
Dardiri, A.H., Bachrach, H.L., Heller, E., 1971. Inhibition by rifampin of African swine fever virus replication in tissue culture. Infect. Immun. 4 (1), 34–36.
Dixon, L.K., Chapman, D.A., Netherton, C.L., Upton, C., 2013. African swine fever virus replication and genomics. Virus Res. 173 (1), 3–14.
Dos Santos Nascimento, I.J., da Silva Rodrigues, E.E., da Silva, M.F, de Araujo-Junior, J. X, de Moura, R.O, 2022a. Advances in computational methods to discover new NS2B-NS3 inhibitors useful against dengue and Zika viruses. Curr. Top. Med. Chem. 22 (29), 2435–2462.
Dos Santos Nascimento, I.J, de Aquino, T.M., da Silva Junior, E.F, 2022b. Computer-aided drug design of anti-inflammatory agents targeting microsomal prostaglandin E (2) synthase-1 (mPGES-1). Curr. Med. Chem. 29 (33), 5397–5419.
Forman, H.J., Torres, M., 2001. Redox signaling in macrophages. Mol. Aspects Med. 22 (4–5), 189–216.
Freitas, F.B., Frouco, G., Martins, C., Leitao, A., Ferreira, F., 2016. In vitro inhibition of African swine fever virus-topoisomerase II disrupts viral replication. Antiviral Res. 134, 34–41.
Galindo, I., Alonso, C., 2017. African swine fever virus: a review. Viruses 9 (5).
Galindo, I., Hernaez, B., Berna, J., Fenoll, J., Cenis, J.L., Escribano, J.M., Alonso, C., 2011. Comparative inhibitory activity of the stilbenes resveratrol and oxyresveratrol on African swine fever virus replication. Antiviral Res. 91 (1), 57–63.
Gao, Q., Yang, L., Zhu, Y., 2010. Pharmacophore based drug design approach as a practical process in drug discovery. Curr. Comput. Aided Drug Des. 6 (1), 37–49.
Garcia-Escudero, R., Garcia-Diaz, M., Salas, M.L., Blanco, L., Salas, J., 2003. DNA polymerase X of African swine fever virus: insertion fidelity on gapped DNA substrates and AP lyase activity support a role in base excision repair of viral DNA. J. Mol. Biol. 326 (5), 1403–1412.
Gil-Fernandez, C., Paez, E., Vilas, P., Gancedo, A.G., 1979. Effect of disodium phosphonoacetate and iododeoxyuridine on the multiplication of African swine fever virus in vitro. Chemotherapy 25 (3), 162–169.
Guner, O.F., 2005. The impact of pharmacophore modeling in drug design. IDrugs 8 (7), 567–572.
Guo, S., Zhang, Y., Liu, Z., Wang, D., Liu, H., Li, L., Chen, Q., Yang, D., Liu, Q., Guo, H., Mou, S., Chen, H., Wang, X., 2023. Brincidofovir is a robust replication inhibitor against African swine fever virus in vivo and in vitro. Emerg. Microbes Infect. 12 (2), 2220572.
Hakobyan, A., Arabyan, E., Avetisyan, A., Abroyan, L., Hakobyan, L., Zakaryan, H., 2016. Apigenin inhibits African swine fever virus infection in vitro. Arch. Virol. 161 (12), 3445–3453.
Hakobyan, A., Arabyan, E., Kotsinyan, A., Karalyan, Z., Sahakyan, H., Arakelov, V., Nazaryan, K., Ferreira, F., Zakaryan, H., 2019. Inhibition of African swine fever virus infection by genkwanin. Antiviral Res. 167, 78–82.
Hakobyan, A., Galindo, I., Nanez, A., Arabyan, E., Karalyan, Z., Chistov, A.A., Streshnev, P.P., Korshun, V.A., Alonso, C., Zakaryan, H., 2018. Rigid amphipathic fusion inhibitors demonstrate antiviral activity against African swine fever virus. J. Gen. Virol. 99 (1), 148–156.
Halim, S.A., Khan, S., Khan, A., Wadood, A., Mabood, F., Hussain, J., Al-Harrasi, A., 2017. Targeting dengue virus NS-3 helicase by ligand based pharmacophore modeling and structure based virtual screening. Front. Chem. 5, 88.
Hernaez, B., Tarrago, T., Giralt, E., Escribano, J.M., Alonso, C., 2010. Small peptide inhibitors disrupt a high-affinity interaction between cytoplasmic dynein and a viral cargo protein. J. Virol. 84 (20), 10792–10801.
Hicks, N.J., Morris, A.G., Burke, D.C., 1981. Partial reversion of the transformed phenotype of murine sarcoma virus-transformed cells in the presence of interferon: a possible mechanism for the anti-tumour effect of interferon. J. Cell Sci. 49, 225–236.
Kapetanovic, I.M., 2008. Computer-aided drug discovery and development (CADDD): in silico-chemico-biological approach. Chem. Biol. Interact. 171 (2), 165–176.
Keita, D., Heath, L., Albina, E., 2010. Control of African swine fever virus replication by small interfering RNA targeting the A151R and VP72 genes. Antivir. Ther. 15 (5), 727–736.
Khedkar, S.A., Malde, A.K., Coutinho, E.C., Srivastava, S., 2007. Pharmacophore modeling in drug discovery and development: an overview. Med. Chem. 3 (2), 187–197.
Lamarche, B.J., Showalter, A.K., Tsai, M.D., 2005. An error-prone viral DNA ligase. Biochemistry 44 (23), 8408–8417.
Lamarche, B.J., Tsai, M.D., 2006. Contributions of an endonuclease IV homologue to DNA repair in the African swine fever virus. Biochemistry 45 (9), 2790–2803.
Laskowski, R.A., Swindells, M.B., 2011. LigPlot+: multiple ligand-protein interaction diagrams for drug discovery. J. Chem. Inf. Model. 51 (10), 2778–2786.
Li, Z., Chen, W., Qiu, Z., Li, Y., Fan, J., Wu, K., Li, X., Zhao, M., Ding, H., Fan, S., Chen, J., 2022. African Swine fever virus: a review. Life (Basel) 12 (8), 1522.
Lin, W.J., 2022. The dawn of a new era in drug discovery? Drug screening and the increasing biological complexity of testing models. Chem. Res. Toxicol. 35 (1), 5–6.
Lopez, E., van Heerden, J., Bosch-Camos, L., Accensi, F., Navas, M.J., Lopez-Monteagudo, P., Argilaguet, J., Gallardo, C., Pina-Pedrero, S., Salas, M.L., Salt, J., Rodriguez, F., 2020. Live attenuated African swine fever viruses as ideal tools to dissect the mechanisms involved in cross-protection. Viruses 12 (12), 1474.
Lu, X., Yang, H., Chen, Y., Li, Q., He, S.Y., Jiang, X., Feng, F., Qu, W., Sun, H., 2018. The development of pharmacophore modeling: generation and recent applications in drug discovery. Curr. Pharm. Des. 24 (29), 3424–3439.
Luo, L., Zhong, A., Wang, Q., Zheng, T., 2021. Structure-based pharmacophore modeling, virtual screening, molecular docking, ADMET, and molecular dynamics (MD) simulation of potential inhibitors of PD-L1 from the library of marine natural products. Mar. Drugs 20 (1), 29.
Monteagudo, P.L., Lacasta, A., Lopez, E., Bosch, L., Collado, J., Pina-Pedrero, S., Correa-Fiz, F., Accensi, F., Navas, M.J., Vidal, E., Bustos, M.J., Rodriguez, J.M., Gallei, A., Nikolin, V., Salas, M.L., Rodriguez, F., 2017. BA71DeltaCD2: a new recombinant live attenuated African swine fever virus with cross-protective capabilities. J. Virol. 91 (21).

Monto, A.S., 2006. Vaccines and antiviral drugs in pandemic preparedness. Emerg. Infect. Dis. 12 (1), 55–60.
Mottola, C., Freitas, F.B., Simoes, M., Martins, C., Leitao, A., Ferreira, F., 2013. In vitro antiviral activity of fluoroquinolones against African swine fever virus. Vet. Microbiol. 165 (1–2), 86–94.
O'Donnell, V., Holinka, L.G., Sanford, B., Krug, P.W., Carlson, J., Pacheco, J.M., Reese, B., Risatti, G.R., Gladue, D.P., Borca, M.V., 2016. African swine fever virus Georgia isolate harboring deletions of 9GL and MGF360/505 genes is highly attenuated in swine but does not confer protection against parental virus challenge. Virus Res. 221, 8–14.
Oliveros, M., Yanez, R.J., Salas, M.L., Salas, J., Vinuela, E., Blanco, L., 1997. Characterization of an African swine fever virus 20-kDa DNA polymerase involved in DNA repair. J. Biol. Chem. 272 (49), 30899–30910.
Paez, E., Garcia, F., Gil Fernandez, C., 1990. Interferon cures cells lytically and persistently infected with African swine fever virus in vitro. Arch. Virol. 112 (1–2), 115–127.
Pirhadi, S., Shiri, F., Ghasemi, J.B., 2013. Methods and applications of structure based pharmacophores in drug discovery. Curr. Top. Med. Chem. 13 (9), 1036–1047.
Qu, H., Ge, S., Zhang, Y., Wu, X., Wang, Z., 2022. A systematic review of genotypes and serogroups of African swine fever virus. Virus Genes 58 (2), 77–87.
Ramirez-Medina, E., Vuono, E., Silva, E., Rai, A., Valladares, A., Pruitt, S., Espinoza, N., Velazquez-Salinas, L., Borca, M.V., Gladue, D.P., 2022. Evaluation of the deletion of MGF110-5L-6L on swine virulence from the pandemic strain of African swine fever virus and use as a DIVA marker in vaccine candidate ASFV-G-DeltaI177L. J. Virol. 96 (14), e0059722.
Redrejo-Rodriguez, M., Garcia-Escudero, R., Yanez-Munoz, R.J., Salas, M.L., Salas, J., 2006. African swine fever virus protein pE296R is a DNA repair apurinic/apyrimidinic endonuclease required for virus growth in swine macrophages. J. Virol. 80 (10), 4847–4857.
Sanchez-Cordon, P.J., Montoya, M., Reis, A.L., Dixon, L.K., 2018. African swine fever: a re-emerging viral disease threatening the global pig industry. Vet. J. 233, 41–48.
Sanchez, E.G., Perez-Nunez, D., Revilla, Y., 2019. Development of vaccines against African swine fever virus. Virus Res. 265, 150–155.
Sang, H., Miller, G., Lokhandwala, S., Sangewar, N., Waghela, S.D., Bishop, R.P., Mwangi, W., 2020. Progress toward development of effective and safe African swine fever virus vaccines. Front. Vet. Sci. 7, 84.
Simoes, M., Martins, C., Ferreira, F., 2013. Host DNA damage response facilitates African swine fever virus infection. Vet. Microbiol. 165 (1–2), 140–147.
Simoes, M., Martins, C., Ferreira, F., 2015a. Early intranuclear replication of African swine fever virus genome modifies the landscape of the host cell nucleus. Virus Res. 210, 1–7.
Simoes, M., Rino, J., Pinheiro, I., Martins, C., Ferreira, F., 2015b. Alterations of nuclear architecture and epigenetic signatures during African swine fever virus infection. Viruses 7 (9), 4978–4996.
Sun, H.P., Zhu, J., Chen, F.H., You, Q.D., 2011. Structure-based pharmacophore modeling from multicomplex: a comprehensive pharmacophore generation of protein kinase CK2 and virtual screening based on it for novel inhibitors. Mol. Inform. 30 (6-7), 579–592.
Tran, X.H., Le, T.T.P., Nguyen, Q.H., Do, T.T., Nguyen, V.D., Gay, C.G., Borca, M.V., Gladue, D.P., 2022a. African swine fever virus vaccine candidate ASFV-G-DeltaI177L efficiently protects European and native pig breeds against circulating Vietnamese field strain. Transbound. Emerg. Dis. 69 (4), e497–e504.
Tran, X.H., Phuong, L.T.T., Huy, N.Q., Thuy, D.T., Nguyen, V.D., Quang, P.H., Ngon, Q. V., Rai, A., Gay, C.G., Gladue, D.P., Borca, M.V., 2022b. Evaluation of the safety profile of the ASFV vaccine candidate ASFV-G-DeltaI177L. Viruses 14 (5).
Tsai, K.C., Hung, P.P., Cheng, C.F., Chen, C., Tseng, T.S., 2019. Exploring the mode of action of inhibitors targeting the PhoP response regulator of Salmonella enterica through comprehensive pharmacophore approaches. RSC Adv. 9 (16), 9308–9312.
Tsai, K.C., Zhang, Y.X., Kao, H.Y., Fung, K.M., Tseng, T.S., 2022. Pharmacophore-driven identification of human glutaminyl cyclase inhibitors from foods, plants and herbs unveils the bioactive property and potential of Azaleatin in the treatment of Alzheimer's disease. Food Funct. 13 (24), 12632–12647.
Tseng, T.S., Chuang, S.M., Hsiao, N.W., Chen, Y.W., Lee, Y.C., Lin, C.C., Huang, C., Tsai, K.C., 2016. Discovery of a potent cyclooxygenase-2 inhibitor, S4, through docking-based pharmacophore screening, in vivo and in vitro estimations. Mol. Biosyst. 12 (8), 2541–2551.
Tulman, E.R., Delhon, G.A., Ku, B.K., Rock, D.L., 2009. African swine fever virus. Curr. Top. Microbiol. Immunol. 328, 43–87.
Tung, M.C., Fung, K.M., Hsu, H.M., Tseng, T.S., 2021a. Discovery of 8-prenylnaringenin from hop (Humulus lupulus L.) as a potent monoacylglycerol lipase inhibitor for treatments of neuroinflammation and Alzheimer's disease. RSC Adv. 11 (49), 31062–31072.
Tung, M.C., Tsai, K.C., Fung, K.M., Don, M.J., Tseng, T.S., 2021b. Characterizing the structure-activity relationships of natural products, tanshinones, reveals their mode of action in inhibiting spleen tyrosine kinase. RSC Adv. 11 (4), 2453–2461.
Urbano, A.C., Ferreira, F., 2022. African swine fever control and prevention: an update on vaccine development. Emerg. Microbes Infect. 11 (1), 2021–2033.
Valasani, K.R., Vangavaragu, J.R., Day, V.W., Yan, S.S., 2014. Structure based design, synthesis, pharmacophore modeling, virtual screening, and molecular docking studies for identification of novel cyclophilin D inhibitors. J. Chem. Inf. Model. 54 (3), 902–912.
Vinuela, E., 1985. African swine fever virus. Curr. Top. Microbiol. Immunol. 116, 151–170.
Wallace, A.C., Laskowski, R.A., Thornton, J.M., 1995. LIGPLOT: a program to generate schematic diagrams of protein-ligand interactions. Protein Eng. 8 (2), 127–134.
Wang, G., Xie, M., Wu, W., Chen, Z., 2021a. Structures and functional diversities of ASFV proteins. Viruses 13 (11).
Wang, N., Zhao, D., Wang, J., Zhang, Y., Wang, M., Gao, Y., Li, F., Wang, J., Bu, Z., Rao, Z., Wang, X., 2019. Architecture of African swine fever virus and implications for viral assembly. Science 366 (6465), 640–644.
Wang, T., Luo, R., Sun, Y., Qiu, H.J., 2021b. Current efforts towards safe and effective live attenuated vaccines against African swine fever: challenges and prospects. Infect. Dis. Poverty 10 (1), 137.
Wang, Y., Kang, W., Yang, W., Zhang, J., Li, D., Zheng, H., 2021c. Structure of African swine fever virus and associated molecular mechanisms underlying infection and immunosuppression: a. Review. Front Immunol. 12, 715582.
Wu, K., Liu, J., Wang, L., Fan, S., Li, Z., Li, Y., Yi, L., Ding, H., Zhao, M., Chen, J., 2020. Current state of global African swine fever vaccine development under the prevalence and transmission of ASF in China. Vaccines (Basel) 8 (3), 531.
Yanez, R.J., Rodriguez, J.M., Nogal, M.L., Yuste, L., Enriquez, C., Rodriguez, J.F., Vinuela, E., 1995. Analysis of the complete nucleotide sequence of African swine fever virus. Virology 208 (1), 249–278.
Yang, S.Y., 2010. Pharmacophore modeling and applications in drug discovery: challenges and recent advances. Drug Discov. Today 15 (11–12), 444–450.
Yoo, D., Kim, H., Lee, J.Y., Yoo, H.S., 2020. African swine fever: etiology, epidemiological status in Korea, and perspective on control. J. Vet. Sci. 21 (2), e38.
Yu, W., MacKerell Jr., A.D., 2017. Computer-aided drug design methods. Methods Mol. Biol. 1520, 85–106.
Zakaryan, H., Revilla, Y., 2016. African swine fever virus: current state and future perspectives in vaccine and antiviral research. Vet. Microbiol. 185, 15–19.
Zhou, Y., Tang, S., Chen, T., Niu, M.M., 2019. Structure-based pharmacophore modeling, virtual screening, molecular docking and biological evaluation for identification of potential poly (ADP-Ribose) polymerase-1 (PARP-1) inhibitors. Molecules 24 (23), 4258.
Zhu, Z., Fan, Y., Liu, Y., Jiang, T., Cao, Y., Peng, Y., 2020. Prediction of antiviral drugs against African swine fever viruses based on protein-protein interaction analysis. PeerJ 8, e8855.
Zoete, V., Grosdidier, A., Michielin, O., 2009. Docking, virtual high throughput screening and in silico fragment-based drug design. J. Cell. Mol. Med. 13 (2), 238–248.